Improved Monitoring of Forest Disturbance and Succession Using an Optimized Satellite Image Index

Matthew Klotzbach
Department of Geography-Geology
Illinois State University
Normal, IL 61790
E-mail: mgklotz@ilstu.edu

Jonathan Thayn
Department of Geography-Geology
Illinois State University
Normal, IL 61790
E-mail: jthayn@ilstu.edu

ABSTRACT

Landscape- to continental-scale studies of forest disturbance and recovery typically rely on satellite image-based indices of vegetation condition. A recently proposed disturbance index that accentuates patches of disturbed forest has been used to detect fire and insect defoliation scars, but until now it has not been used to assess recovery over time. We used a weighted version of the index to emphasize canopy differences caused by fire while minimizing other differences that may exist in the imagery to monitor succession following the 1988 fires in Yellowstone National Park. Spectral estimates of moisture levels were the most important difference between burned and unburned patches, while differences in estimates of photosynthetic activity were weak and decreased as succession progressed. Burned areas were clearly highlighted in the weighted images. Classifications based on the weighted index were reliably accurate, although they gradually decreased as succession erased the difference between disturbed and undisturbed forest. The weighted index successfully reduced the effects of differences that were not the focus of the research; the weights in particular helped maintain the sensitivity of the disturbance index through Yellowstone's recovery.

Key Words: Disturbance Index, forest fire recovery, forest succession, greenness, lodgepole pine, Yellowstone National Park

INTRODUCTION

Identifying and mapping ecosystem disturbances is an important task made more efficient through the use satellite imagery, especially at regional to continental scales. Recently, Healey et al. (2005) proposed a new image-processing technique, which they call the Disturbance Index (DI), that highlights forested areas that have been recently disturbed. The DI has been successfully

used to detect disturbance caused by insects (Deel et al. 2012; DeRose et al. 2011; Has et al. 2009; Wulder et al. 2006), logging and windfall (Dyukarev et al. 2011; Rick et al. 2010), armed conflict (Gorsevski et al. 2012), and to map continental-scale disturbances regardless of the cause (Masek et al. 2008). The DI has also been used to assess the effects of disturbance on the nitrogen cycle (Dyukarev et al. 2011; McNeil et al. 2007) and to detect disturbance caused by the construction of new Walmart locations (Potere et al. 2008).

The DI is simple to calculate and interpret, but possibly its most useful advantage is that it can be fitted to specific disturbances and locations using weighting coefficients (Healey et al. 2005). In this way, disturbances of interest can be highlighted while minimizing other differences that may be present in the image, such as those caused by atmospheric or climate change (Thayn 2013). This has not been assessed over time, as the forest recovers from the disturbance. In the current paper, we address the following key questions: (1) Do the weighting coefficients help the DI remain sensitive to disturbances even as recovery progresses, and (2) Does the weighted DI help reduce confusion between disturbed sites and areas that are naturally less verdant? We also began to assess qualitatively whether changes in the derived weights might reflect changes in biophysical conditions as succession progresses, although additional research and field work are required to fully assess this relationship.

Images collected by satellite remote sensing systems record relative measurements of solar energy reflectance, which can be used reliably as surrogates for vegetation condition. Kauth and Thomas (1976) and Crist and Kauth (1986) introduced a linear transform of satellite imagery, called the Tasseled Cap Transform (TCT), that converts satellite imagery into estimates of relative brightness (overall reflectivity), greenness (the amount of photosynthesis occurring), and wetness (including moisture held in soil or in foliage). Healey et al. (2005) recognized that brightness increases and greenness and wetness decrease in forested pixels that have been disturbed, and suggested that disturbed areas could be highlighted by subtracting the sum of the greenness and wetness values from the brightness value: DI = B - (G + W). DeRose et al. (2011) used this Disturbance Index (DI) to identify insect-caused mortality of Engelmann Spruce trees (*Picea engelmannii*) and noted that map accuracy increased with the severity of the disturbance.

Healey et al. (2005) suggested that weighting the TCT components (brightness, greenness, and wetness) before calculating the DI might improve its ability to detect forest disturbances. Weighting the TCT values would fit the DI to local conditions and accentuate the disturbance of interest while dampening other differences that may be present in the forest canopy or in the satellite data. Thayn (2013) used a weighted DI, which he called an optimized DI (DIopt), to map insect defoliation in deciduous forests in northern Wisconsin: $DIopt = w_1B - (w_2G + w_3W)$, where w_1, w_2, and w_3 are weighting coefficients which are used to emphasize the TCT components that are more useful for detecting disturbance. Thayn found that disturbance detection was consistently better with the weighted DI than with the unweighted DI (2013).

In this paper, we report on a study of the recovery of the 1988 fires in Yellowstone National Park. The accuracy of disturbance detection was assessed quantitatively by comparing the results to a burn scar outline prepared and provided by the Yellowstone Spatial Analysis Laboratory (YSAL, 2013). Also, we compare our results qualitatively to the work of Turner and her colleagues (Turner et al. 1997, 1999, 2003, 2004) who have conducted extensive field work in Yellowstone related to fire recovery. We make this comparison only to provide context for our results and as a sort of qualitative accuracy assessment. We do not attempt to draw conclusions about specific ecological processes.

METHODS

We downloaded one cloud-free summertime image for each year from 1988 to 2003 from the USGS Global Visualization website (GLOVIS, 2014). This time-series allowed us to examine 15 years of recovery time, which was sufficient to assess the value of weighting the DI. We attempted to select images from the same time of year (late summer to early fall) to avoid confusing seasonal change with successional change; however, extensive cloud coverage in some of these images pushed a few of our dates into early October. Imagery from the Thematic Mapper (TM) and Enhanced Thematic Mapper plus (EMT+) sensors aboard Landsat 4, 5, and 7 were used. We also used a vector Geographic Information System (GIS) outline of the 1988 fire produced and distributed by the Yellowstone Spatial Analysis Laboratory (YSAL 2013).

The images were converted to the brightness, greenness, and wetness TCT component bands (Crist and Kauth 1986; Huang et al. 2002). Each TCT component was then converted to a z-score (Rogerson 2004 p. 7) by subtracting from each pixel value the mean of healthy forest pixels and dividing the result by the standard deviation of healthy forest pixels. We used a random point generator that placed points outside of the burn scar outline prepared by YSAL to collect the sample of healthy forest values from which the mean and standard deviation were calculated. We reviewed these sample points to ensure that no points fell on roadways, water bodies, grasslands or other non-forest locations. Converting the TCT components to z-scores in this way effectively transformed them to their distance, in tasseled cap feature space, from healthy forest. For example, a pixel with a positive number in the z-score greenness band would be more green than healthy forest, a pixel with a negative number would be less green than healthy forest, and a pixel with a z-score near zero would be just as green as healthy forest (see Table 1 in Thayn 2013). The further a pixel's z-score is from zero, the further it is from typical healthy forest, making interpretation of the z-scores intuitive and simple.

The second, and most important reason the TCT components were converted to z-scores was to normalize the ranges of the components so that they were essentially equivalent. The original equation for the DI assumes that the three TCT components are of equal importance in identifying disturbed vegetation. If one component was composed of numbers that were twice as large as those of the other components, it would carry twice the weight of the other components. Converting the TCT components to z-scores gives each component the same spread of values and eliminates these hidden, unintended weights. Also, the z-score calculation is similar to dark object subtraction in that it can limit the effects of relatively homogenous atmospheric noise (Huang et al. 2010), so that other atmospheric correction may not be required (DeRose et al. 2011, Song et al. 2001).

To derive the weights for calculating the optimized DI, we randomly selected 364 training points from within the YSAL burn scar outline and 381 points from outside of the burn boundary. Each point was carefully examined to ensure that it fell on burned or unburned forest cover, not some other landcover. The TCT z-scores associated with these training points were submitted to an iterative Nelder-Mead optimization that maximized the chi-squared statistic of a Kruskal-Wallace test, just as in Thayn (2013). The Nelder-Mead technique is a widely popular nonlinear downhill approach to finding a local, unimodal solution (Bélisle 1992; Lagarias et al. 1998). It is particularly useful for problems involving multiple interdependent variables, like the brightness, greenness, and wetness TCT components (Nelder and Mead 1965). The optimization was done using the "optim" function of the R statistical software (R Core Team 2012).

The Kruskal-Wallace test is a nonparametric, one-way analysis of variance based on the sums of samples' observations' ranks that is used to determine whether samples belong to

Table 1: Estimates of the area burned along with user's accuracy, producer's accuracy, and overall accuracy with 95% confidence intervals.

		User's Accuracy		Producer's Accuracy		
Year	Burned Area	Not Burned	Burned	Not Burned	Burned	Overall Accuracy
1988	561.83 ± 35.30	0.68 ± 0.05	0.92 ± 0.04	0.95 ± 0.02	0.59 ± 0.04	0.76 ± 0.03
1989	575.72 ± 37.33	0.63 ± 0.05	0.93 ± 0.04	0.96 ± 0.02	0.50 ± 0.03	0.71 ± 0.03
1990	597.48 ± 39.43	0.67 ± 0.05	0.86 ± 0.04	0.90 ± 0.03	0.56 ± 0.04	0.73 ± 0.03
1991	560.35 ± 39.28	0.60 ± 0.05	0.84 ± 0.05	0.90 ± 0.03	0.46 ± 0.03	0.67 ± 0.04
1992	565.30 ± 39.49	0.61 ± 0.05	0.81 ± 0.05	0.87 ± 0.03	0.49 ± 0.03	0.67 ± 0.04
1993	594.37 ± 36.37	0.68 ± 0.05	0.90 ± 0.04	0.93 ± 0.03	0.61 ± 0.04	0.76 ± 0.03
1994	579.66 ± 36.56	0.70 ± 0.05	0.89 ± 0.04	0.91 ± 0.03	0.64 ± 0.04	0.77 ± 0.03
1995	602.62 ± 40.35	0.64 ± 0.05	0.85 ± 0.05	0.90 ± 0.03	0.52 ± 0.03	0.71 ± 0.03
1996	601.35 ± 38.57	0.67 ± 0.05	0.85 ± 0.04	0.89 ± 0.03	0.61 ± 0.04	0.74 ± 0.03
1997	599.06 ± 39.43	0.67 ± 0.05	0.80 ± 0.05	0.82 ± 0.04	0.63 ± 0.04	0.72 ± 0.03
1998	596.13 ± 39.92	0.66 ± 0.05	0.79 ± 0.05	0.82 ± 0.03	0.62 ± 0.04	0.72 ± 0.04
1999	605.18 ± 41.62	0.62 ± 0.05	0.79 ± 0.05	0.86 ± 0.03	0.50 ± 0.03	0.68 ± 0.04
2000	570.60 ± 39.63	0.61 ± 0.05	0.78 ± 0.05	0.82 ± 0.04	0.56 ± 0.04	0.68 ± 0.04
2001	597.97 ± 41.71	0.65 ± 0.05	0.76 ± 0.05	0.82 ± 0.03	0.56 ± 0.04	0.69 ± 0.04
2002	571.20 ± 41.10	0.61 ± 0.05	0.77 ± 0.05	0.84 ± 0.03	0.50 ± 0.04	0.66 ± 0.04
2003	562.50 ± 41.13	0.64 ± 0.05	0.74 ± 0.05	0.79 ± 0.03	0.57 ± 0.04	0.68 ± 0.04

the same distribution (Kruskal and Wallace 1952). Our data were not normally distributed so using a parametric test would have been inappropriate. The Nelder-Mead optimization progressively changed the weighting coefficients and performed a Kruskal-Wallis test on the weighed TCT z-score data until a maximum chi-squared statistic was returned, indicating that the differences between the burned and unburned training samples had been maximized. The set of coefficients that returned the largest chi-statistic was then used to weight the images. This process was repeated for each year's image so that different weights were found for each year.

After masking the water bodies from the DIopt images, we classified each pixel as burned or unburned forest using a maximum likelihood classifier with training data sampled independently of the locations used to derive the weights. Finally, we performed accuracy assessments for each year in the analysis using the equations provided by Olofsson et al. (2013). The reference data for the accuracy assessment were created by overlaying the GIS outline of the burn scar provided by the Yellowstone Spatial Analysis Laboratory with 671 points created using a random point generator. Three hundred and fifty-two of these points fell within the burn scar, and 319 fell outside its boundary. These classes (burned or unburned) were assumed to be accurate and were used as the reference data.

RESULTS

This discussion of our results begins with a qualitative visual comparison of the yearly weighted DI images. Context is provided by

referring to the published research of other scientists, mostly that of Dr. Monica G. Turner and her colleagues, whose research was based on extensive field work in the Yellowstone 1988 burn area. This is followed by quantitative accuracy assessments of each year's classification results and a corresponding discussion. Modeling specific plant conditions or drawing conclusions about biological processes is beyond the scope of this study, which is designed only to assess the sensitivity of the weighted DI over time. An analysis based on more thorough ground reference data is the next step in this research program.

Figure 1a shows the unweighted DI image for 1988, just after the fires were extinguished, while Figure 1b shows the weighted DIopt image calculated from the same image. In both of these images, lighter areas show locations which were more likely to have been burned, while darker areas were more likely to have not been burned. Notice in the unweighted image (Fig. 1a) that location 1 (Hayden Valley) and location 2 (Pitchstone Plateau) were both very light, suggesting that these areas were burned, when in fact they were not. Hayden Valley is a grassland area whose vegetation was more spectrally similar to recovering burnt forest (possibly with a rapidly growing understory) than to undisturbed forest. Pitchstone Plateau is a rhyolite lava flow whose relatively sparse vegetation was also spectrally more similar to recovering burnt forest than to dense forest. The weighted DIopt image, Figure 1b, accurately displays these areas as unburned. We were careful to collect data from locations in the Hayden Valley and Pitchstone Plateau areas when deriving the weights to ensured that these areas were "trained" as unburned locations. Forest recovery was evident in the 1994 DIopt image (Figure 1c). In the northwest of the study site, near Madison (location 3), and along the Central Plateau (location 4) the 1994 image appeared darker (less disturbed or more recovered) than it appeared in the 1988 image (Figure 1b). This was also true, to a lesser degree, around Grant Village (location 5). Turner et al. (2003) report that within a year of the fire, this area was covered with herbs, grasses, and shrubs. Sapling density of serotinous lodgepole pines (*Pinus contorta*) increased immediately after the fire (Turner et al. 2004), especially in older stands (Schoennagel et al. 2003). The percentage of Lodgepole pine saplings that reach mature height was higher in 1990 and was greater in severe-surface burns rather than in areas that experienced crown fires (Turner et al. 1999). Also in 1990, aspen (*Populus tremuloides*) were identified in burned lodgepole pine forests (Turner et al. 1997). Fireweed (*Epilobium angustifolium*) flowered abundantly in 1990 and peaked in 1991 when it formed thick patches of waist-high stems (Turner et al. 1997).

Lightly burned areas returned to their pre-fire percent vegetative cover by 1991 and severely burned areas had recovered half of their percent cover by 1992, even though shrub cover was still reduced (Turner et al. 1999). By 1993, percent cover of tree saplings, primarily lodgepole pine, had reached 10.0% in the northwest, less than 1.0% in the southwest, and less than 0.1% in the southeast near Yellowstone Lake (Turner et al. 1997). Percent forb cover had increased in the southwest and southeast but not in the northwest while shrub cover was still uniformly low across all burned areas (Turner et al. 1997). Canada thistle (*Cirsium arvense*) was increasing in 1993 when Turner et al. (1997) finished collecting field data, and it likely continued to increase for some time. All of this new, post-fire growth is evident in the 1994 weighted DI image.

Eleven years after the fire, in 1999 (Figure 1d), approximately 66% of the burned areas had stand densities of less than 5000 saplings per ha, but 25% of the burned area had densities greater than 10,000 saplings per ha and about 7% had densities exceeding 50,000 saplings per ha (Turner et al. 2004). Most of the high-density stands were located in the north of the study site, near the Central Plateau (location 4) while most of the low-density stands were south of Yellowstone

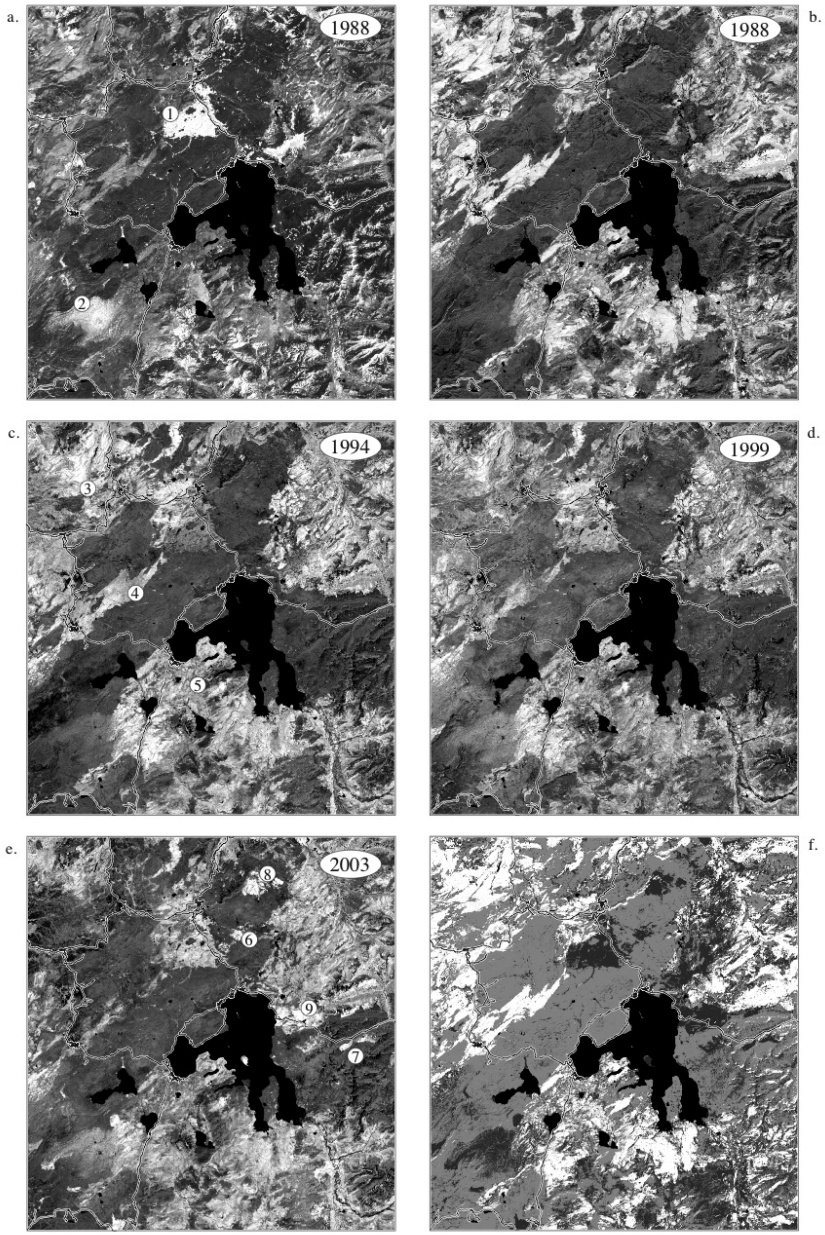

Figure 1: Image a shows the DI of the 1988 YNP study area. Images b, c, d, and e portray the DIopt from 1988, 1994, 1999, and 2003, respectively; note that a number of brighter patches show up in e, representing new forest fires which occurred between 2001-2003. Image f contrasts the 1988 and 2003 optimized images: areas which displayed some recovery by 2003 are displayed in white; patches in dark gray indicate areas that were more burnt/ disturbed in 2003 than in 1988; light gray patches did not change over time.

Lake. The low-density of lodgepole stands south of Yellowstone Lake was due to the greater fire severity in that area. The more rapid recovery in the north of Yellowstone compared to the south is evident in the 1999 DIopt image.

By 2003, many of the lighter areas in the DIopt image had darkened and some had disappeared, indicating significant recovery of burned areas since 1988 (Figure 1e). The Central Plateau region (location 4) and areas northward showed the most dramatic improvement. This was consistent with trends outlined in the literature cited earlier. Recovery south of Yellowstone Lake occurred much more slowly. Based on field data collected in 1993, Turner et al. (1997) concluded that post-fire reestablishment in the Yellowstone Lake area was questionable, with fewer than 10 seedlings observed per ha in the area. Seedling viability of the lodgepole pine species is generally less than five years, while it is less than three years for the Engelmann spruce and less than 1 year for the subalpine fir. It is possible, then, that the window for reestablishment of these species has been missed in the south and that some of the area south of Yellowstone Lake (which remained lighter in our 2003 DIopt image) may not return to its pre-fire forest condition but become a grasslands region similar to Hayden Valley (Turner et al. 1997).

Several more recent fires appeared as lighter spots in the 2003 DIopt image (Figure 1e), such as the Sulfur and Arthur Fires (locations 6 and 7) which both occurred in 2001. The Broad and East Fires (locations 8 and 9) occurred in 2003, as did the fire on Frank Island in Yellowstone Lake. The more recent burn scars appeared in the temporal composite image as well (Figure 1f). In this image, areas whose weighted DI was greater in 1988, indicating recovery, are displayed in white. Areas with lower weighted DI values in 2003 are showing in dark gray – these are areas that are more disturbed in 2003 than they were in 1988, or locations of newer fires. Areas displayed in light gray are those whose weighted DI is essentially the same in 2003 as they were in 1988.

The weights used to create the DIopt images varied only slightly over time (Fig. 2). The means of each TCT component's weights, with their standard deviation in parentheses, were: brightness, -5.77 (2.67); greenness, 0.67 (2.56); and wetness, 8.78 (1.46). Since the TCT components were normalized as z-scores, these weights are relative to one another, i.e., the brightness component was about 8.5 times more important than greenness, and wetness was about 1.5 times more important than brightness. Wetness,

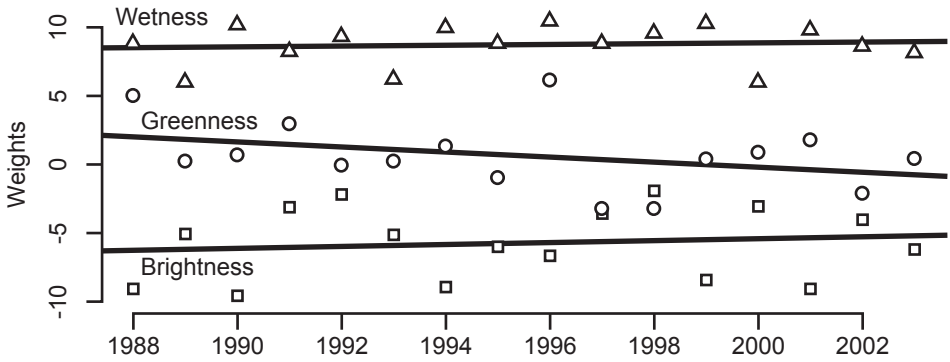

Figure 2: The weights for each TCT component for each year of the 16-year study period. The importance of Wetness was positive, suggesting that burned areas did not recover their pre-fire ability to retain moisture. Brightness was negative and decreases in importance over time. Greenness was the least important and gradually declines as succession progresses.

then, was the most important TCT component for distinguishing between burned and unburned forest canopy. Brightness was also important while greenness was the least important component.

The wetness components' weights were positive, suggesting that burned areas were drier than unburned areas, although this was not verified with field data. It seems that over the course of this 16-year time-series, the burned areas did not recover their pre-fire ability to retain moisture. It is likely that some patches of bare soil and ash persist on the landscape, which would make the pixels that contain them appear spectrally to be drier than pixels that are covered with dense vegetation.

Comparisons of brightness TCT component values for burned areas were slightly larger than those of unburned forest. Accordingly, the weights for the brightness component were negative. This was contrary to the expectation outlined by Healey et al. (2005), possibly because the burned areas quickly filled with fast growing grasses and forbs (Turner et al. 1997) and so appeared to be covered with healthy vegetation. These plants absorb sunlight to power photosynthesis, thereby reducing reflectivity. However, it was unknown why the reflectivity of these areas would be lower than that of the unburned forest, although differences in species compositions could be partly responsible.

Greenness was the least important component for discerning between burned and unburned forest, likely because burned areas were quickly filled with perennial herbs, grasses, and shrubs which "flowered profusely" (Turner et al. 2003 p. 353). The positive mean weight for greenness suggests that the unburned sites were more photosynthetically active than the burned sites, but only slightly. Notice that the importance of greenness decreased with succession (its weights trend toward zero over time in Figure 2). The trend line for greenness' weights reached zero between 2000 and 2001, suggesting that for this fire, and for this satellite-based measure of photosynthetic activity, the burned areas had recovered their photosynthetic productivity by that time.

The size of the area burned, including 95% confidence intervals, was estimated for each year of the study using the equations of Olofsson et al. (2013). Naturally, the extent of the disturbed area would not change, but the detectable area, or our confidence in its detection, might decrease if the DI loses sensitivity to the disturbance as recovery progresses. The area of the detected burn scar did not change statistically from year to year as recovery progressed ($F = 0.386$, $p = 0.544$) – its mean was 583.83 ± 39.20 thousand acres. Even after 15 years of succession, the full extent of the burn scar was detectable using the weighted DI. Each year's DI image was created using weights that accentuated the difference between the unburned and the burned forest for each years' condition. The weights changed to emphasize areas that had been burned, so the DIopt highlighted the burned areas despite subsequent recovery. However, the size of the 95% confidence intervals of the area estimates increased from 35.30 thousand acres the year after the fire to 41.13 thousand acres 15 years later, and this increase was statically significant ($F = 17.07$, $p = 0.001$). While our estimates of the burned area did not change over time, our confidence in those estimates slowly eroded.

The user's accuracy is an estimate of the probability that a pixel classified as burned was truly burned. A low user's accuracy for burned pixels would suggest a high commission error rate, i.e., that many unburned pixels were incorrectly classified as burned. The producer's accuracy is an estimate of the probability that a burned location in the field was correctly classified. Low producer's accuracy for burned pixels would suggest that many burned areas escaped detection, or a high omission error rate. Our discussion of classification accuracy will focus only on the burned class, since that is the focus of this work and the accuracy of the unburned class is simply the reverse of the burned class.

The producer's accuracies for burned sites ranged from 0.46 to 0.64, with a mean of 0.56 ± 0.03, suggesting that some burned locations escaped detection. These were likely slightly burned locations that, from a spectral reflectance perspective, have more in common with healthy forest than disturbed forest. It is quite possible that the understory of these slightly burned areas grew quickly. A verdant understory would be more spectrally similar to healthy forest than to burned forest and might confuse the classification algorithm. Unfortunately, we do not have access to field data from 1989 that might verify this. The producer's accuracy of burned areas did not vary predictably from year to year ($F = 0.13$, $p = 0.722$), so any pixels that were only slightly disturbed (thus escaping detection) in 1989 remained undetectable through 2003.

Users accuracy for burned locations decreased from 0.92 in 1989 to 0.74 in 2003, so we can be very confident that any pixel classified as burned represents a location that was actually burned. Very few unburned sites were incorrectly classified as burned. However, the decrease in the users accuracy of the burned class was statistically significant ($F = 46.91$, $p < 0.000$), suggesting that as recovery progressed, burned locations began to appear spectrally more like unburned locations, and the classification began to confuse the two classes. This happened even though the DIopt images had been fitted to each year's condition using the weighting coefficients.

The overall accuracy of the classification, including both the burned and the unburned classes, started at 0.76 ± 0.03 and declined to 0.68 ± 0.04 after 15 years of recovery. This decrease was statistically significant ($F = 4.26$, $p = 0.058$). Most of the overall classification errors were the slightly disturbed sites that escaped detection, as mentioned above. The large majority of pixels that were classified as burned were correctly identified. Like all methods for detecting recovering disturbance sites, however, the DIopt becomes increasingly unable to identify burned pixels as recovery progresses.

DISCUSSION

The first question this project was designed to address was whether the weighting coefficients of the DI help it to remain sensitive to disturbances as recovery progresses, and our results suggest that it does. Classifications of the weighted DI were able to detect the full extent of the 1988 fires, even after 15 years of succession and recovery. This was even true in areas that were less severely burned. The detected area of the burn scar was statistically unchanged from year to year; however, 95% confidence intervals of the detected area increased over time, suggesting that our confidence in the weighted DI decreased with recovery. As recovering forest regains some of its initial condition, the burn scar will be more and more difficult to detect, and while statistically weighting the DI increases its sensitivity, the burn scar will eventually be erased from the landscape, at least spectrally. Until then, weighting the DI seems to increase the likelihood that researchers will be able to successfully map past disturbances.

The second question addressed by this project is whether weighting the DI reduces confusion between disturbed and naturally less productive locations. Again, our results suggest that it does. This is possibly the most useful aspect of the weighting the DI. It can fit the index to specific disturbances of interest while dampening or weakening the effects of other differences that are not as important to the researcher. This possibility was suggested by Healey et al. (2005) but was not demonstrated in that paper. In the present paper, we demonstrate that some of the less verdant regions of Yellowstone National Park, like the Hayden Valley grasslands and the Pitchstone Plateau, were initially classified as burned forest. The classification based on the weighted DI was able to recognize that they were not burned locations, but areas that were more spectrally similar to burned forests than to unburned forest. This property of the weighted DI makes it appealing for studies of disturbances in multiple landuse study sites.

The advantages of the weighted DI come with a cost. First, the researcher must be able to identify locations of disturbed and undisturbed forest canopy. If this is not possible, e.g., if the researcher is trying to locate previously unknown disturbances, than the unweighted DI is the best option. Also, there is a considerable increase in processing time, especially when deriving the weights.

As we experimented with deriving the weights, we realized that the optimization solution was not unimodal, i.e., there were multiple potential solutions. A maximizing Nelder-Mead optimization moves iteratively to larger values until movement in any direction decreases the statistic. In this way, finding the largest statistic, indicative of the best solution, is like climbing a mountain. If every step you take is uphill, you will eventually reach the top. From there, every direction is downhill and the optimization stops. When the solution is not unimodal, it is as if there were multiple mountain peaks in the same area. The problem is that the optimization will climb to the top of a mountain and stop, but there may be a taller peak, or a better solution, nearby (Nelder and Mean 1965). In a non unimodal scenario, the Nelder-Mead optimization may stop at a local maximum and ignore the global maximum that represents a better solution.

The solution to this problem is to carefully start the optimization on the foothills of the tallest mountain and not on those of one of the shorter peaks. From our initial work we were confident that the optimum weights would be greater than -10 and less than 10, so we found the chi-statistic for every combination of integer weights within that range. The combination of weights with the largest chi-statistic was then used as the starting point in the Nelder-Mead optimization. The disadvantage of this approach is increased computation time and complexity. With 21 possible integer weights between -10 and 10 for each of three weights, over 9,000 Kruskal-Wallis tests were needed to find the starting point for the optimization. A more sophisticated optimization technique, one designed for multi-modal solutions, could have been more efficient. Despite this, the Nelder-Mead optimization was very useful for weighting the DIopt, which proved very useful for clearly distinguishing disturbed areas and areas recovering from disturbance.

ACKNOWLEDGMENTS

This research was partly funded by the National Science Foundation, award number 1339927.

REFERENCES

Bélisle, C. J. P. 1992. Convergence Theorems for a Class of Simulated Annealing Algorithms on R^d. *Journal of Applied Probability*, 29: 885-895.

Crist, E. P., and Cicone, R. C. 1984. A Physically-Based Transformation of Thematic Mapper Data – The TM Tasseled Cap. *IEEE Transactions on Geoscience and Remote Sensing,* GE-22: 256-263.

Crist, E.P., and Kauth, R.J. 1986. The Tasseled Cap De-mystified. *Photogrammetric Engineering and Remote Sensing,* 52: 81-86.

Deel, L. N., McNeil, B. E., Curtis, P. G., Serbin, S. P., Singh, A., Eshleman, K. N., & Townsend, P. A. 2012. Relationship of a Landsat Cumulative Disturbance Index to Canopy Nitrogen and Forest Structure. *Remote Sensing of Environment,* 118(0): 40-49. doi: [http://dx.doi.org/10.1016/j.rse.2011.10.026].

DeRose, R. J., Long, J. N., and Ramsey, R. D. 2011. Combining Dendrochronological Data and the Disturbance Index to Assess Engelmann Spruce Mortality Caused by a Spruce Beetle Outbreak in Southern Utah, USA. *Remote Sensing of Environment,* 115: 2342-2349.

Dyukarev, E. A., Pologova, N. N., Golovatskaya, E. A., & Dyukarev, A. G. 2011. Forest Cover Disturbances in the South Tiaga of West Siberia. *Environment Research Letters, 6*(3): 035203 (9 pages).

GLOVIS, USGS. 2014. [http://glovis.usgs.gov/index.shtml]. Last accessed on 7 July 2014.

Gorsevski, V., Kasischke, E., Dempewolf, J., Loboda, T., and Grossmann, F. 2012. Analysis of the Impacts of Armed Conflict on the Eastern Afromontane Forest Region on the South Sudan - Uganda Border Using Multitemporal Landsat Imagery. *Remote Sensing of Environment,* 118(0): 10-20. doi: [http://dx.doi.org/10.1016/j.rse.2011.10.023].

Hais, M., Jonášová, M., Langhammer, J., and Kučera, T. 2009. Comparison of Two Types of Forest Disturbance Using Multitemporal Landsat TM/ETM+ Imagery and Field Vegetation Data. *Remote Sensing of Environment,* 113(4): 835-845. doi: [http://dx.doi.org/10.1016/j.rse.2008.12.012].

Healey, S. P., Cohen, W. B., Zhiqiang, Y., and Krankina, O. N. 2005. Comparison of Tasseled Cap-based Landsat Data Structures for Use in Forest Disturbance Detection. *Remote Sensing of Environment,* 97: 301-310.

Huang, C., Goward, S. N., Masek, J. G., Thomas, N., Zhu, Z., and Vogelmann, J. E. 2010. An Automated Approach for Reconstructing Recent Forest Disturbance History Using Dense Landsat Time Series Stacks. *Remote Sensing of Environment,* 114: 183-198.

Huang, C., Wylie, B., Yang, L., Homer, C., and Zylstra, G. 2002. Derivation of a Tasseled Cap Transformation Based on Landsat 7 At-Satellite Reflectance. *International Journal of Remote Sensing*, 23(8): 1741-1748.

Kauth, R. J., and Thomas, G. S. 1976. The Tasseled Cap – A Graphical Description of the Spectral-Temporal Development of Agricultural Crops as Seen by Landsat. Proceedings of the *Symposium on Machine Processing of Remotely Sensed Data*; Purdue University, West Lafayette, Indiana.

Kruskal, W. H. & Wallis, W. A. 1952. Use of Ranks in One-Criterion Variance Analysis. *Journal of the American Statistical Association,* 47(260): 583-621.

Lagaris, J. C., Reeds, J. A., Wright, M. H. & Wright, P. E. 1998. Convergence Properties of the Nelder-Mead Simplex Optimization Method in Low Dimensions. *SIAM Journal on Optimization*. 9: 112-147.

Masek, J. G., Huang, C., Wolfe, R., Cohen, W., Hall, F., Kutler, J., & Nelson, P. 2008. North American Forest Disturbance Mapped from a Decadal Landsat Record. *Remote Sensing of Environment,* 112(6), 2914-2926. doi: [http://dx.doi.org/10.1016/j.rse.2008.02.010].

McNeil, B. E., de Beurs, K. M., Eshleman, K. N., Foster, J. R., and Townsend, P. A. 2007. Maintenance of Ecosystem Nitrogen Limitation by Ephemeral Forest Disturbance: An Assessment Using MODIS, Hyperion, and Landsat ETM+. *Geophys. Res. Lett.,* 34(19): L19406. doi: [10.1029/2007gl031387].

Nelder, J. A., and Mead, R. 1965. A Simplex Method for Function Minimization. *The Computer Journal,* 7: 308-313.

Olofsson, P., Foody, G. M., Stehman, S. V., and Woodcock, C. E. 2013. Making Better Use of Accuracy Data in Land Change Studies: Estimating Accuracy and Area and Quantifying Uncertainty Using Stratified Estimation. *Remote Sensing of Environment* 129: 122-131.

Potere, D., Felerabend, N., Strahler, A. H., and Bright, E. A. 2008. Wal-Mart from Space: A New Source for Land Cover Change Validation. *Photogrammetric Engineering and Remote Sensing,* 74(7): 913-919.

R Core Team. 2012. R: A Language and Environment for Statistical Computing. R Foundation for Statistical Computing, Vienna, Austria.

Rich, R. L., Frelich, L., Reich, P. B., and Bauer, M. E. 2010. Detecting Wind Disturbance Severity and Canopy Heterogeneity in Boreal Forest by Coupling High-Spatial Resolution Satellite Imagery and Field Data. *Remote Sensing of Environment,* 114(2): 299-308. doi: [http://dx.doi.org/10.1016/j.rse.2009.09.005].

Rogerson, P.A. 2004. Statistical Methods for Geography. Sage Publications. ISBN: 0-7619-6288-3.

Schoennagel, T., Turner, M. G., and Romme, W. H. 2003. The Influence of Fire Interval and Serotiny on Postfire Lodgepole Pine Density in Yellowstone National Park. *Ecology*, 84: 2967-2978.

Song, C., Woodcock, C. E., Seto, K. C., Lenney, M. P., and Macomber, S. A. 2001. Classification and Change Detection Using Landsat TM Data: When and How to Correct Atmospheric Effects? *Remote Sensing of Environment,* 75: 230-244.

Thayn, J. B. 2013. Using a Remotely Sensed Optimized Disturbance Index to Detect Insect Defoliation in the Apostle Islands, Wisconsin, USA. *Remote Sensing of Environment,* 136: 210-217.

Turner, M. G., Romme, W. H., and Gardner, R. H. 1999. Prefire Heterogeneity, Fire Severity, and Early Postfire Plant Reestablishment in Subalpine Forests of Yellowstone National Park, Wyoming. *International Journal of Wildland Fire,* 9: 21-36.

Turner, M.G., Romme, W. H., Gardner, R. H., and Hargrove, W. W. 1997. Effects of Fire Size and Pattern on Early Succession in Yellowstone National Park. *Ecological Monographs,* 67: 411-433.

Turner, M. G., Romme, W. H., and Tinker, D. B. 2003. Surprises and Lessons from the 1988 Yellowstone Fires. *Frontiers in Ecology and the Environment*, 1: 351-358.

Turner, M. G., Tinker, D. B., Romme, W. H., Kahian, D. M., and Litton, C. M. 2004. Landscape Patterns of Sapling Density, Leaf Area, and Aboveground Net Primary Production in Postfire Lodgepole Pine Forests, Yellowstone National Park (USA). *Ecosystems,* 7: 751-775.

Wulder, M. A., White, J. C., Bentz, B., Alvarez, M. F., and Coops, N. C. 2006. Estimating the Probability of Mountain Pine Beetle Red-Attack Damage. *Remote Sensing of Environment,* 101(2): 150-166. doi: [http://dx.doi.org/10.1016/j.rse.2005.12.010].

YSAL. 2013. Yellowstone Spatial Analysis Laboratory. [http://www.nps.gov/yell/naturescience/spatialanalysiscenter.htm]. Last accessed 24 July 2013.